RSC Advances

ROYAL SOCIETY OF CHEMISTRY

www.rsc.org/advances

RSC Advances

ARTICLE

Radiosynthesis and evaluation of *N*-(3,4-dimethylisoxazol-5-yl)piperazine-4-[4-(4-fluorophenyl)thiazol-2-yl]-1-[11C]carboxamide for in vivo positron emission tomography imaging of fatty acid amide hydrolase in brain

Y. Shimoda,[a] J. Yui,[a] Y. Zhang,[a] A. Hatori,[a] M. Ogawa,[a] M. Fujinaga,[a] T. Yamasaki,[a] L. Xie,[a] K. Kumata,[a] M.-R. Zhang[a],*

We developed a novel positron emission tomography (PET) radiotracer *N*-(3,4-dimethylisoxazol-5-yl)piperazine-4-[4-(4-fluorophenyl)thiazol-2-yl]-1-[11C]carboxamide ([11C]DPFC, [11C]**1**) for *in vivo* imaging of fatty acid amide hydrolase (FAAH) in rat brain. Compound **1** showed a high binding affinity for FAAH (IC_{50}: 3.3 nM). [11C]**1** was synthesized by reaction of 5-amino-3,4-dimethylisoxazole (**2**) with [11C]phosgene ([11C]$COCl_2$), followed by reaction with 4-(4-fluorophenyl)-2-(piperazin-1-yl)thiazole (**3**), with a 9 ± 4% radiochemical yield (decay-corrected, $n = 9$) based on [11C]CO_2. A biodistribution study in mice showed a high uptake of radioactivity in FAAH-rich organs, including the lung, liver, and kidney. PET summation images of rat brains showed high radioactivity (> 2 SUV) in the cerebellar nuclei and frontal cortex. This pattern was consistent with the known regional distribution pattern of FAAH in the rodent brain. Pretreatment with the FAAH-selective inhibitor URB597 significantly reduced the whole brain uptake of [11C]**1**. At 30 min after the radiotracer injection, more than 95% of the total radioactivity was found to be irreversible in the brain homogenate of rats. Our results indicate that [11C]**1** is a promising PET tracer for in vivo visualization of FAAH in living brains.

Introduction

Fatty acid amide hydrolase (FAAH) is an intracellular serine hydrolase that catalyzes the deactivating hydrolysis of several endogenous lipid amides, such as oleamide, an endogenous ligand that induces sleep, and anandamide, an endogenous ligand that activates cannabinoid receptors.[1-3] The lipid properties of anandamide indicates that this signaling molecule cannot be stored in vesicles, unlike most polar G-protein coupled receptors.[4,5] In the central nervous system, the level of anandamide is primarily regulated by FAAH.[6,7] Selective inhibitors of FAAH were found to show marked pharmacological effects on pain, anxiety, addiction, and in psychiatric disorders.[8-10] Moreover, FAAH inhibitors may provide anti-inflammatory effects by suppressing the release of inflammatory chemical mediators through stimulation of the cannabinoid type 2 receptor in immune cells.[11] Because of their pharmacological effects, and because they cause few adverse actions, many FAAH inhibitors have been developed; structurally, these are urea, carbamate, and keto-heterocycle derivatives.[12]

Recently, there has been increasing interest in the development of radiotracers for in vivo positron emission tomography (PET) imaging of FAAH in living brain. To our knowledge, there are only two such PET tracers used for clinical studies. [11C]CURB (Fig. 1), an irreversible inhibitor of FAAH,[13] is the first useful imaging agent, and has been used for quantitative measurement of FAAH in human

brain.[14,15] Given the success of [11C]CURB, several research groups have embarked on developing alternative PET tracers and elucidating relationships among the chemical structure, the in vitro binding affinity, and the in vivo specificity of such agents for FAAH.[16-21] Most of the promising PET tracers contain a [11C-carbonyl]carbamate or [11C-carbonyl]urea unit and are characterized as irreversible FAAH inhibitors. In addition to the irreversible tracers, the use of [11C]MK-3168 (Fig. 1), a reversible inhibitor for FAAH, is also being studied in human subjects.[22]
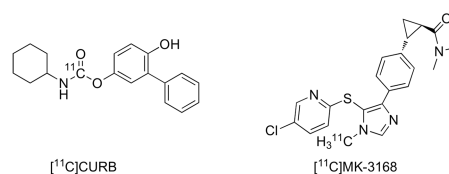

Fig. 1. Chemical structures of PET radiotracers for imaging FAAH in clinical use.

We have previously developed [11C]MFTC (Fig. 2) containing an [11C-carbonyl]carbamate moiety, for in vivo imaging of FAAH in rat and monkey brains.[23] [11C]MFTC showed high specific binding for FAAH in rodent brains. However, the presence of considerable non-

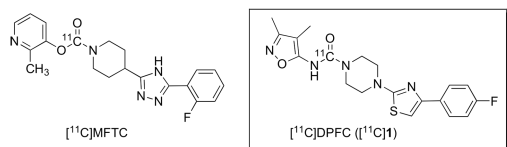specific binding of this radiotracer in the monkey brain hindered the application of [11C]MFTC in clinical studies.[23]

Fig. 2. Chemical structures of irreversible radiotracers for FAAH labeled by [11C]COCl2.

In this study, we developed *N*-(3,4-dimethylisoxazol-5-yl)piperazine-4-[4-(4-fluorophenyl)thiazol-2-yl]-1-[11C]carboxamide ([11C]DPFC, [11C]**1**, Fig. 2) as a new radiotracer for imaging of FAAH. We radiosynthesized [11C]**1** using [11C]phosgene ([11C]COCl2) as a labeling agent. We then evaluated potential of [11C]**1** for in vivo PET imaging of FAAH by determining in vitro binding affinity for FAAH, biodistribution, brain uptake, and in vivo specific irreversible binding in the rat brain.

Results and discussion

Targeted Compound

In this study, we selected compound **1** as a new candidate for PET imaging of brain FAAH, based on the following considerations. This compound showed potent in vitro binding affinity for FAAH (IC50 = 0.86 nM for human and 0.71 nM for rat FAAH).[24,25] It has been reported that **1** shows a moderate brain uptake of 132 ng/g at 1 h after intravenous injection of 0.1 mg/kg into rats.[24] This finding suggested that [11C]**1** may achieve adequate brain uptake while imaging FAAH in the brain. A suitable computed lipophilicity (clogD) value of 3.15 for [11C]**1** could support this suggestion. On the other hand, compound **1** containing a urea moiety could be considered as an irreversible inhibitor of FAAH that binds covalently to the catalytic Ser241 residue within the active site of the FAAH protein.[13] Furthermore, compound **1** can be labeled with [11C]COCl2, without changing its chemical structure and pharmacological profile.

Radiolabeling

Regarding the chemical structure of **1** with an unsymmetrical urea moiety, we labeled **1** by reacting two different amines: 5-amino-3,4-dimethylisoazole (**2**) and 4-(4-fluorophenyl)-2-(piperazin-1-yl)thiazole (**3**), with [11C]COCl2 (Fig. 3).
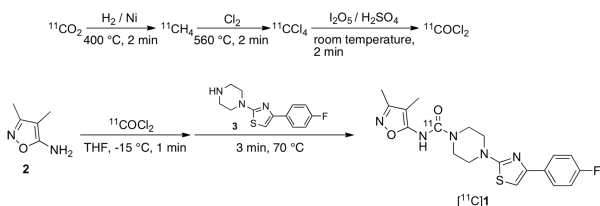

Fig. 3. Radiosynthesis of [11C]**1** using [11C]COCl2 as a labeling agent.

[11C]COCl2 was synthesized from cyclotron-produced [11C]CO2 via [11C]CH4 and then via [11C]CCl4 using a home-made automated production system (Fig. 3).[27-29] The produced [11C]COCl2 gas was bubbled into a solution of amine precursor **2** at −15 °C for 1 min, followed by another reaction with amine precursor **3** at 70 °C for 3

min. A low temperature is required for the first reaction of **2** with [11C]COCl2; if the reaction was performed at 20 °C, the reaction would mainly produce the symmetrical [11C]urea of **2**. After optimizing the conditions for reacting [11C]COCl2 with amine **2** and then amine **3** was optimized, a completely automated synthesis of [11C]**1** was carried out. The reaction mixture was then separated by high performance liquid chromatography (HPLC, Fig. 4a) to obtain the final product. Starting with 18.5–26.6 GBq of [11C]CO2, 0.4–1.1 GBq of [11C]**1** was obtained at the end of synthesis (*n* = 9). The average total synthesis time, from the end of bombardment, was 36 min.
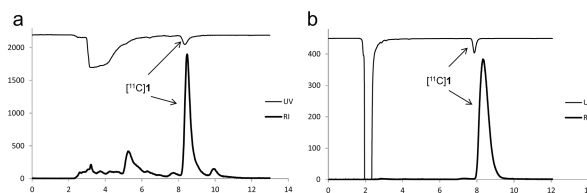

Fig. 4. Chromatograms from the HPLC separation (a) and analysis (b) of [11C]**1**. See Experimental Section for the chromatographic conditions.

The identity of [11C]**1** was confirmed by co-injection with unlabeled compound **1** on analytic HPLC (Fig. 4b). In the final product solutions, the radiochemical purity of [11C]**1** was higher than 98% and specific activity was 23–66 GBq/μmol (*n* = 9). No significant UV peak representing chemical impurity was seen on the HPLC charts of finally-formulated products. Moreover, the radiochemical purity of [11C]**1** remained >95% after 90 min at room temperature, and this product was radiochemically stable for the period of one PET scan. These analytical results were in compliance with the quality control/assurance specifications established in our laboratory.

In Vitro Binding Assays

Compound **1** has previously been reported to show high in vitro binding affinity for FAAH (IC50: 0.86/0.71 nM for human/rat FAAH). Here, we used competitive activity-based protein profiling[16,23] to confirm the in vitro potency of **1** for FAAH. Fig. 5 shows the binding curves of **1**, and URB597 as a control, for FAAH in rat brain homogenate. The in vitro binding affinity (IC50) of **1** for FAAH was calculated from these curves as 3.3 ± 1.0 nM, while that
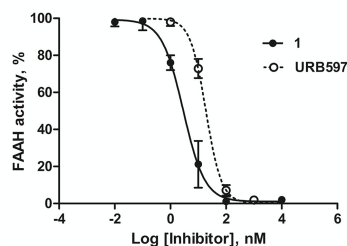
Fig. 5. In vitro binding assay of compound **1** and URB597 for FAAH. Two compounds were incubated at different concentrations (10^−2–10^4 nM). Percentages (*n* = 3, means ± s.d.) of specific binding indicated inhibition of test compounds against FAAH.

of URB597 was 19.6 ± 3.5 nM. Under the same experimental conditions, compound **1** was characterized as showing 6-fold and 4-fold higher binding affinity than URB597 or MFTC (IC50: 13.6 nM[23]), respectively. This result indicated that the binding affinity of **1** was sufficient for PET imaging of FAAH in the brain.

Biodistribution Study

The distribution of radioactivity in whole body of mice was measured at different time points after injection of $[^{11}C]$**1** (Table 1). At 1 min, high uptake (> 2% ID/g) was observed in the blood, brain, heart, liver, lung, kidney, and small intestine. After the initial phase, the radioactivity in the blood and heart decreased rapidly and remained low until the end of the experiment, while the radioactivity in the lung, small intestine, spleen, and kidney continued to increase until 15–30 min and then decreased. The liver uptake increased within the period of this experiment. On the other hand, a high initial uptake of radioactivity (3.07% ID/g) at 1 min after the injection was found in the mouse brain and the brain uptake slowly increased to 4.01% ID/g by 60 min.

Table 1. Distribution of Radioactivity in Mice after Injection of $[^{11}C]$1^a

tissue	1 min	5 min	15 min	30 min	60 min
blood	3.26 ± 0.62	0.74 ± 0.10	0.28 ± 0.02	0.18 ± 0.02	0.14 ± 0.01
heart	7.32 ± 0.59	1.40 ± 0.05	0.48 ± 0.03	0.40 ± 0.04	0.32 ± 0.05
lungs	17.79 ± 2.75	13.00 ± 4.25	12.89 ± 4.59	12.60 ± 1.68	9.56 ± 3.00
liver	9.43 ± 1.79	18.07 ± 2.23	23.75 ± 1.41	22.47 ± 3.67	22.49 ± 3.31
spleen	2.67 ± 0.69	3.28 ± 0.47	3.28 ± 1.03	3.87 ± 0.39	2.30 ± 0.38
kidneys	26.62 ± 2.87	32.06 ± 3.06	38.97 ± 1.00	39.03 ± 2.75	36.00 ± 3.57
small intestine	6.34 ± 0.91	9.53 ± 1.35	10.39 ± 0.43	10.54 ± 1.04	10.00 ± 1.41
testes	0.68 ± 0.08	0.90 ± 0.13	0.90 ± 0.08	0.95 ± 0.09	1.01 ± 0.08
muscle	2.96 ± 0.29	0.85 ± 0.13	0.27 ± 0.05	0.16 ± 0.02	0.13 ± 0.05
brain	3.07 ± 0.14	3.54 ± 0.24	3.29 ± 0.21	3.74 ± 0.12	4.01 ± 0.32

^{a}Data are % ID/g tissue (mean ± SD; n = 4).

It has been reported that FAAH is enriched in the brain, liver, kidney, and lung, but not in the muscle and hearts of rodents.[31-34] Our present results indicated that the radioactivity distribution of $[^{11}C]$**1** was in agreement with the distribution of FAAH and was also similar to the distribution patterns of $[^{11}C]$CURB and $[^{11}C]$MFTC in the corresponding mouse regions.[13,23] The considerable brain uptake demonstrated that $[^{11}C]$**1** can pass through the blood-brain barrier rapidly, which is an indispensable prerequisite for a useful PET tracer in brain imaging. The brain uptake of $[^{11}C]$**1** may be related to its suitable lipophilicity (cLogD: 3.15) and the lack of significant interaction of $[^{11}C]$**1** with the efflux function of the blood-brain barrier. In mouse brain in the present study, the radioactivity level slightly increased after the injection up to 60 min, suggesting that $[^{11}C]$**1** may have some irreversible binding in the brain, although the uptake indicates slow kinetics.

PET Study in Rats

Fig. 6 shows representative PET images of rat brains after injection of $[^{11}C]$**1** (Fig. 6a) and $[^{11}C]$**1** pretreated with 3 mg/kg URB597 (Fig. 6b). The control PET images exhibited considerable brain entrance and accumulation of radioactivity in the rat brain (Fig. 6a). The highest radioactivity was seen in the cerebellar nucleus, followed by the frontal cortex, cerebellar cortex, hippocampus, striatum, and thalamus, while the lowest uptake was observed in the pons. As shown in the time-activity curves (TACs) of the brain regions (Fig. 7a), the radioactivity entered the brain and distributed throughout the regions immediately after the injection, and slightly increased from 10 min until the end of the PET scans. As shown on the PET images (Fig. 6b) and TACs (Fig. 7b), pretreatment with URB597 markedly reduced the uptake in the control brains. Pretreatment caused the radioactivity levels at 90 min to be reduced by 50–80% within all
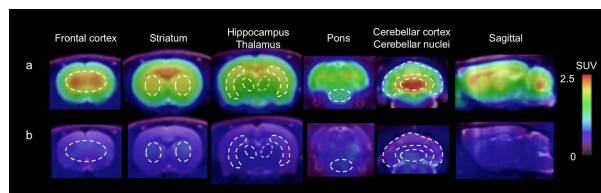

Fig. 6. Representative coronal and sagittal PET/MRI images for $[^{11}C]$**1** in rat brains (*n* = 4 for each group). (a) $[^{11}C]$**1** only. (b) Pretreatment with URB597.
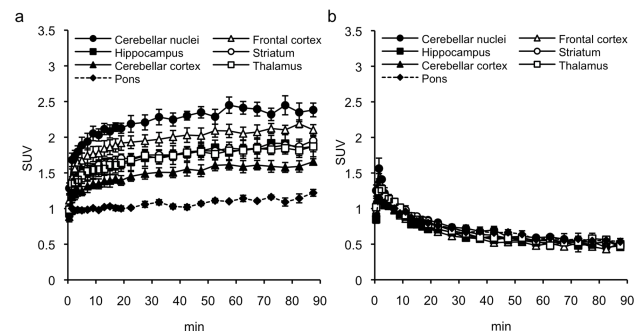

Fig. 7. Time-activity curves for $[^{11}C]$**1** in rat brains (*n* = 4 for each group). (a) $[^{11}C]$**1** only. (b) Pretreatment with URB597.

brain regions; and the maximum reduction (about 80% reduction) was found in the cerebellar nucleus. The radioactivity distribution became regionally homogeneous with a low uptake level.

The PET results indicated that the distribution pattern of $[^{11}C]$**1** reflects the distribution of FAAH in the rat brain[31-34] and was similar to that of $[^{11}C]$MFTC.[23] Significant inhibition by the FAAH-selective URB597 demonstrated that $[^{11}C]$**1** has specific binding targets in the rat brain. Because both of **1** and URB597 showed high in vitro binding specificity for FAAH in the brain, we concluded that the in vivo specific binding of $[^{11}C]$**1** determined in this study could be ascribed to FAAH.

Measurement of the Irreversible Binding

By measuring the radioactivity in the extracts and residual pellets which were separated from the rat brains, the percentages of $[^{11}C]$**1** bound to rat brain tissue were assessed (Table 2). At 5 min after injection, 97% of total radioactivity in the brain homogenate was found to irreversibly bind to brain tissue and this was retained at 98% at 30 min. Specificity of $[^{11}C]$**1** for the in vivo irreversible binding to FAAH was confirmed by performing the same procedure in rats pretreated with URB597. As shown in Table 2, the treatment virtually completely abolished the irreversible binding with only 0.7% and 2% of total radioactivity remaining in the brain tissue at 5 and 30 min after the injection. The extraction experiments demonstrated that $[^{11}C]$**1** irreversibly bound to FAAH in the rat brain.

Table 2.   Percentage (%) of $[^{11}C]$1 Bound to Rat Brain Tissue after Injection

Time (min)	mean	±	S.D
5	97.23	±	0.24
30	98.32	±	0.41
pretreatment with URB597			
5	0.70	±	0.13
30	2.04	±	0.53

In the present study, PET with $[^{11}C]$**1** visualized FAAH and demonstrated in vivo specific binding of $[^{11}C]$**1** for FAAH in the rat

brain. Moreover, the in vivo binding was characterized as being irreversible in the brain. These results were in accordance with the properties of an irreversible PET radiotracer, such as [11C]CURB[13] and [11C]MFTC[23], useful for imaging brain FAAH. A limitation for this new PET tracer is its slow kinetics in the brain. After the injection of [11C]1, the brain uptake of [11C]1 continuously increased until the end of the PET scan and did not reach an equilibrium state. This kinetics may cause some difficulty in the quantitative measurement of FAAH in the living brain. This problem may be solved by decreasing the lipophilicity of 1. We are currently optimizing its chemical structure to derive new compounds with decreased lipophilicity while maintaining its potent binding affinity for FAAH and to obtain more suitable PET tracers than [11C]1 for imaging and quantitative measurement of FAAH.

Conclusions

In this study, we have developed [11C]1 as a novel radiotracer for PET imaging of FAAH in brain. PET studies of rat brains with [11C]1 showed relatively high radioactivity uptake and specific binding to FAAH in the brains. [11C]1 is thus a promising radiotracer for visualizing FAAH in the brain.

Experimental
Materials and methods
All chemicals and solvents were of analytic or HPLC grade and were obtained from Aldrich (Milwaukee, WI) and Tokyo Chemical Industries (Tokyo, Japan). Authentic compound 1 and an amine precursor, 4-(4-fluorophenyl)-2-(piperazin-1-yl)thiazole (3), were synthesized according to the procedures reported previously.[24] The lipophilicity of 1 at pH 7.4 (cLogD) was calculated with ADMET Predictor (Simulationsplus, Lancaster, CA). Carbon-11 was produced by ^{14}N(p, α)^{11}C nuclear reaction using a CYPRIS HM18 cyclotron (Sumitomo Heavy Industry, Tokyo, Japan). A dose calibrator (IGC-3R Curiemeter, Aloka, Tokyo) was used to measure radioactivity unless otherwise stated. Reverse phase HPLC was performed using a JASCO system (JASCO, Tokyo, Japan). Effluent radioactivity was measured using a NaI (Tl) scintillation detector system.

Radiosynthesis of [11C]1

After irradiation, the cyclotron-produced [11C]CO_2 was recovered from the cyclotron target with N_2 and converted to [11C]CH_4 by transferring through a heated methanizer (400 °C) filled with nickel catalysts. [11C]CH_4 was mixed with chlorine gas at 560 °C to produce [11C]CCl_4, which was continuously passed through a glass tube containing iodine oxide and sulfuric acid (Kitagawa gas detection tube, Komyo Rikagaku Kogyo, Kawasaki, Japan) at room temperature to produce [11C]$COCl_2$. The obtained [11C]$COCl_2$ flowed into a solution of 2 (0.6 mg) in tetrahydrofuran (THF, 500 μL) at −15 °C for 1 min. After trapping of [11C]$COCl_2$ was completed, 3 (1.3 mg) in THF (300 μL) was added, and the reaction mixture was heated at 70 °C for 3 min.

After removal of THF, the reaction mixture was separated by means of semi-preparative HPLC on a Capcell Pak UG80 C_{18} column (10 mm internal diameter × 250 mm, Shiseido, Tokyo, Japan) and MeCN/H_2O/trifluoroacetic acid (50/50/0.1) was used as mobile phase at a flow rate of 5.0 mL/min. The radioactive fraction corresponding to [11C]1 (retention time: 8.5 min) was collected in a sterile flask, evaporated to dryness in vacuo, redissolved in 3 mL of sterile normal saline, and passed through a 0.22-μm Millipore filter (Billerica, MS) to obtain [11C]1. The identity of the product was

confirmed by coinjecting this radioactive product with authentic 1 on an analytic HPLC (Capcell Pak UG80 C_{18} column, 4.6 mm × 250 mm), using MeCN/H_2O/trifluoroacetic acid (50/50/0.1) as mobile phase at a flow rate of 1.0 mL/min (retention time: 8.3 min). The specific activity was calculated by comparing the assayed radioactivity to the mass measured at UV 254 nm.

Animal Experiments
All animal experiments were performed according to the recommendations of the Committee for the Care and Use of Laboratory Animals, National Institute of Radiological Sciences. Animals were maintained and handled in accordance with the recommendations of the National Institute of Health and institutional guidelines of the National Institute of Radiological Sciences. Mice (ddy, male; 7-weeks-old; weight: 34–36 g) and rats (Sprague-Dawley male; 7-weeks-old; weight: 210–230 g) were purchased from Japan SLC (Shizuoka, Japan). These animals were housed under a 12-h dark/light cycle and were allowed free access to food pellets and water.

In Vitro Binding Affinity

The binding affinity (IC_{50}) for FAAH was assessed according to a previously published procedure using competitive activity-based protein profiling.[16,23] Briefly, membrane fractions (50 μL, 1 mg/mL total protein concentration) of rat brain homogenate were preincubated with varying concentrations (0.01 nM-10 μM) of 1 or URB597 for 30 min at 37 °C. A fluorophosphonate-rhodamine probe (1 μL, 50 μM in DMSO) was added and the reaction mixture was incubated for 30 min at 37 °C. The reaction was stopped by addition of SDS loading buffer. The reaction mixtures were developed on an SDS-PAGE gel, and displayed using a Fluor Image Analyzer FLA-5100 (GE Healthcare, Little Chalfont, UK). Fluorescence of the relevant band at each concentration of inhibitor (1 or URB597) was measured. Concentration-response curves were fit with GraphPad Prism 5 software (GraphPad Software, La Jolla, CA) to calculate the IC_{50} values.

Biodistribution Study in Mice
A saline solution of [11C]1 (2 MBq, 0.05 nmol/200 μL) was injected into mice through the tail vein. Four mice were sacrificed by cervical dislocation at 1, 5, 15, 30, and 60 min after the injection. Blood, whole brain, heart, lung, liver, spleen, kidneys, small intestine, muscle, and testes samples were quickly removed and weighed. The radioactivity accumulated in these tissues was measured using a 1480 Wizard gamma counter (Perkin-Elmer Japan, Yokohama, Japan), and expressed as percent of the injected dose per gram of wet tissue (% ID/g). All radioactivity measurements were corrected for decay.

Small-Animal PET Study in Rat Brains

All PET scans were performed using a small-animal Inveon PET scanner (Siemens Medical Solutions USA, Knoxville, TN), which provides 159 transaxial slices 0.796-mm apart (center-to-center), a 10-cm transaxial field of view (FOV), and a 12.7-cm axial FOV. Prior to the scans, rats were anesthetized with 5% (v/v) isoflurane, and maintained thereafter with 1–2% (v/v) isoflurane. The emission scans were conducted for 90 min after the intravenous injection of [11C]1 (17 ± 3 MBq, 0.45–0.70 nmol). For the pretreatment study, the FAAH-selective inhibitor URB597 (3 mg/kg) was dissolved in saline containing 10% ethanol and 5% Tween 80, and this solution administered to the animals 30 min before the injection of [11C]1 (17 ± 2 MBq, 0.40–0.53 nmol).

All list-mode acquisition data were sorted into 3-dimensional sinograms, which were then Fourier rebinned into 2-dimensional sinograms (frames × min: 4 × 1, 8 × 2, 14 × 5). Dynamic images were reconstructed with filtered back-projections using a Ramp's filter and a Nyquist cutoff of 0.5 cycles/pixel. Regions of interest (ROIs) were placed on the frontal cortex, striatum, thalamus, hippocampus, cerebellar cortex, cerebellar nuclei, and pons using ASIPro VM (Siemens Medical Solutions, Malvern, PA) with reference to a template magnet resonance image (MRI) of a rat brain. PET images were obtained by summing the radioactivity uptake between 0–90 min after the injection of [^{11}C]**1**. Each PET image was overlaid onto the MRI, and a time-activity curve (TAC) for each brain region was acquired. Brain uptake of radioactivity was decay-corrected to the injected time and expressed as the standardized uptake value (SUV) and normalized for injected radioactivity and body weight; SUV was calculates as SUV = (radioactivity per cubic centimeter tissue/injected radioactivity) × gram body weight.

Determination of Irreversible Binding in the Brains

This experiment was performed according to a previously described protocol.[13] Briefly, after intravenous injection of [^{11}C]**1** (37 MBq, 0.68–0.84 nmol/200 μL) into rats, the rats were sacrificed at 5 or 30 min (n = 3 for each time point), respectively. Whole brain samples were removed quickly. For the inhibitory study, URB597 (3 mg/kg) was administered 30 min before the injection of [^{11}C]**1** (37 MBq, 0.74–0.82 nmol). The URB597-treated rats (n = 3) were also sacrificed at 5 or 30 min, respectively. The whole brains of all experimental rats were individually homogenized in 2.5 mL of ice-cold 80% MeCN/20% water and centrifuged (15,000 × g, 10 min, 4 °C). The supernatants were carefully decanted and the pellets were resuspended in the same volume of extraction solvent. This procedure was repeated twice. The pellet and all supernatants from each rat were counted for radioactivity, respectively. The radioactivity in the pellet and all supernatants from each rat was counted.

ACKNOWLEDGEMENTS

Notes and references

[a] Molecular Imaging Centre, National Institute of Radiological Sciences, Inage-ku, Chiba 263-8555, Japan.

[b] SHI Accelerator Service Co. Ltd, Shinagawa-ku, Tokyo 141-8686, Japan.

1 B. F. Cravatt, B. K. Giang, S. P. Mayfield, D. L. Boger, R. A. Lerner and N. B. Gilula, *Nature*, 1996, **384**, 83.

2 D. K. Giang and B. F. Cravatt *Proc. Natl. Acad. Sci. U. S. A.*, 1997, **94**, 2238.

3. N. Ueda, R. A. Puffenbarger, S. Yamamoto and D. G. Deutsch, *Chem. Phys. Lipids.*, 2000, **108**, 107.

4 D. Piomelli, The molecular logic of endocannabinoid signaling. *Nature Rev. Neurosci.*, 2003, **4**, 873.

5 F. Rodríguez de Fonseca, M. Navarro, R. Gómez, L. Escuredo, F. Nava, J. Fu, E. Murillo-Rodríguez, A. Giuffrida, J. LoVerme, S. Gaetani, S. Kathuria, C. Gall and D. Piomelli, *Nature*, 2001, **414**, 209.

6 D. L. Boger, S. J. Henriksen and B. F. Cravatt, *Curr. Pharm. Des.*, 1998, **4**, 303.

7 T. Bisogno, L. De Petrocellis and V. Di Marzo, *Curr. Pharm. Des.* 2002, **8**, 533.

8 L. A. Batista, P. H. Gobira, T. G. Viana, D. C. Aguiar and F. A. Moreira, *Behav. Pharmacol.*, 2014, **25**, 425.

9 M. Sałaga, M. Sobczak and J. Fichna, *Eur. J. Pharm. Sci.*, 2014, **52**, 173.

10 B. P. Roques, M. C. Fournié-Zaluski and M. Wurm, *Nat. Rev. Drug Discov.*, 2012, **11**, 292.

11 I. K. Khanna and C. W. Alexander, *CNS Neurol. Disord. Drug Targets* 2011, **10**, 545.

12 M. Seierstad and J. G. Breitenbucher, *J. Med. Chem.*, 2008, **51**, 7327.

13 A. A. Wilson, A, Garcia, J. Parkes, S. Houle, J. Tong and N. Vasdev N. *Nucl. Med. Biol.*, 2011, **38**, 247.

14 P. M. Rusjan, A. A. Wilson, R. Mizrahi, I. Boileau, S. E. Chavez, N. J. Lobaugh, S. J. Kish, S. Houle and J. Tong, *J. Cereb. Blood Flow Metab.*, 2013, **33**, 407.

15 I. Boileau, R. F. Tyndale, B. Williams, E. Mansouri, D. J. Westwood, B. Le Foll, P. M. Rusjan, R. Mizrahi, V. De Luca, Q. Zhou, A. A. Wilson, S. Houle, S. J. Kish and J. Tong, *J. Cereb. Blood Flow Metab.* 2015, **35**, 1237.

16 M. B. Skaddan, L. Zhang, D. S. Johnson, A. Zhu, K. R. Zasadny, R. V. Coelho, K. Kuszpit, G. Currier, K. H. Fan, E. M. Beck, L. Chen, S. E. Drozda, G. Balan, M. Niphakis, B. F. Cravatt, K. Ahn, T. Bocan and A. Villalobos, *Nucl. Med. Biol.* 2013, **40**, 1058.

17 A. A. Wilson, J. W. Hicks, O. Sadovski, J. Parkes, J. Tong, S. Houle, C. J. Fowler and N. Vasdev. *J. Med. Chem.* 2013, **56**, 201.

18 J. W. Hicks, J. Parkes, O. Sadovski, J. Tong, S. Houle, N. Vasdev and A. A. Wilson, *Nucl. Med. Biol.* 2013, **40**, 740.

19 O. Sadovski, J. W. Hicks, J. Parkes, R. Raymond, J. Nobrega, S. Houle, M. Cipriano, C. J. Fowler, N. Vasde and A. A. Wilson, *Bioorg. Med. Chem.* 2013, **21**, 4351.

20 M. K. Pandey, T. R. DeGrado, K. Qia, M. S. Jacobson, C. E. Hagen, P. I. Jr. Duclos, S. J. Gatley, *ACS Chem. Neurosci.*, 2014, **5**, 793.

21 B. H. Rotstein, H. Y. Wey, T. M. Shoup, A. A. Wilson, S. H. Liang, J. M. Hooker and N. Vasdev, *Mol. Pharm.*, 2014, **11**, 3832.

22 P. Liu, T. G. Hamill, M. Chioda, H. Chobanian, S. Fung, Y. Guo, L. Chang, R. Bakshi, Q. Hong, J. Dellureficio, L. S. Lin, C. Abbadie, J. Alexander, H. Jin, S. Mandala, L. L. Shiao, W. Li, S. Sanabria, D. Williams, Z. Zeng, R. Hajdu, N. Jochnowitz, M. Rosenbach, B. Karanam, M. Madeira, G. Salituro, J. Powell, L. Xu, J. L. Terebetski, J. F. Leone, P. Miller, J. Cook, M. Holahan, A. Joshi, S, O'Malley, M. Purcell, D. Posavec, T. B. Chen, K. Riffel, M. Williams, R. Hargreaves, K. A. Sullivan, R. P. Nargund and R. J. DeVita, *ACS Med. Chem. Lett.*, 2013, **4**, 509.

23 K. Kumata, J. Yui, A. Hatori, L. Xie, M. Ogawa, T. Yamasaki, Y. Nagai, Y. Shimoda, M. Fujinaga, K. Kawamura and M.-R. Zhang, *ACS Chem. Neurosci.*, 2015, **6**, 339.

24 M. Kono, T. Matsumoto, T. Kawamura, A. Nishimura, Y. Kiyota, H. Oki, J. Miyazaki, S. Igaki, C. A. Behnke, M. Shimojo and M. Kono, *Bioorg. Med. Chem.*, 2013, **21**, 28.

25 M. Kono, T. Matsumoto, T. Imaeda, T. Kawamura, S. Fujimoto, Y. Kosugi, T. Odani, Y. Shimizu, H. Matsui, M. Shimojo and M. Kono, *Bioorg. Med. Chem.*, 2014, **22**, 1468.

26 V. W. Pike, *Trends Pharmacol. Sci.* 2009, **30**, 431.

27 M. Ogawa, Y. Takada, H. Suzuki, K. Nemoto and T. Fukumura, *Nucl. Med. Biol*., 2010, **37**, 73.

28 Y. Takada, M. Ogawa, H. Suzuki and T. Fukumura, *Appl. Radiat. Isot*., 2010, 68, 1715.

29 C. Asakawa, M. Ogawa, K. Kumata, M. Fujinaga, K. Kato, T. Yamasaki, J. Yui, K. Kawamura, A. Hatori, T. Fukumura and M.-R. Zhang, *Bioorg. Med. Chem. Lett.,* 2011, **21**, 2220.

30 K. Nishijima, Y. Kuge, K. Seki, K. Ohkura, N. Motoki, K. Nagatsu, A. Tanaka, E. Tsukamoto, N. Tamaki, *Nucl. Med. Biol.* 2002, **29**, 345.

31 K. Watanabe, H. Ogi, S. Nakamura, Y. Kayano, T. Matsunaga, H. Yoshimura and I. Yamamoto, *Life Sci*., 1998, **62**, 1223.

32 C. Fowler, K. O. Jonsson and G. Tiger. *Biochem. Pharmacol*. 2001, **62**, 517.

33 C. J. Hillard, D. M. Wilkison, W. S. Edgemond and W. B. Campbell, *Biochem. Biophys. Acta*., 1995, **1257**, 249.

34 E. A. Thomas, B. F. Cravatt, P. E. Danielson, N. B. Gilula and J. G. Sutcliffe, *J. Neurosci. Res*., 1997, **50**, 1047.